Supplementary Information

β-(Z)-Selective Alkyne Hydrosilylation by a N,O-Functionalized NHC-based Rhodium(I) Catalyst

Miguel González-Lainez, M. Victoria Jiménez,* Vincenzo Passarelli, and Jesús J. Pérez-Torrente*

Departamento de Química Inorgánica – Instituto de Síntesis Química y Catálisis Homogénea-ISQCH, Universidad de Zaragoza – CSIC, C/ Pedro Cerbuna 12, 50009 Zaragoza, Spain

Contents

1.- NMR spectra of rhodium(I) organometallic compounds 2-6.

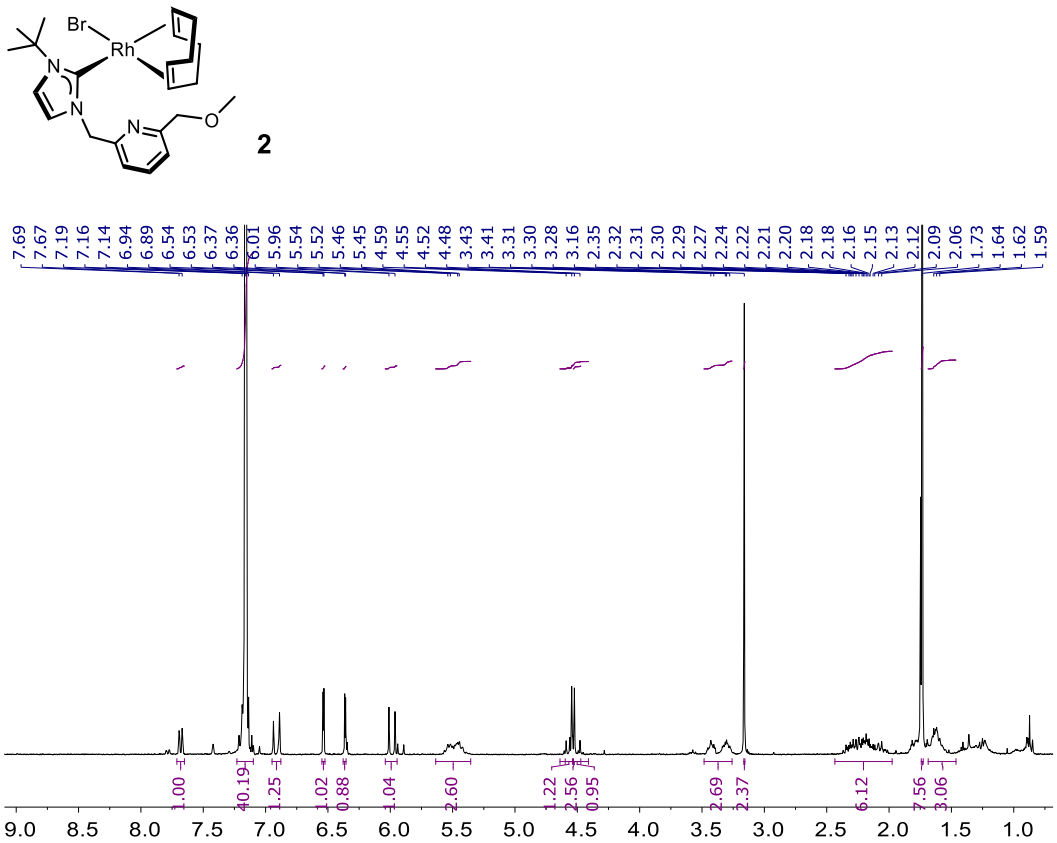

Figure S1. ^{1}H NMR (C_6D_6) spectrum of [RhBr(cod)(κ*C*-^{t}BuImCH$_2$PyCH$_2$OMe)] (**2**).

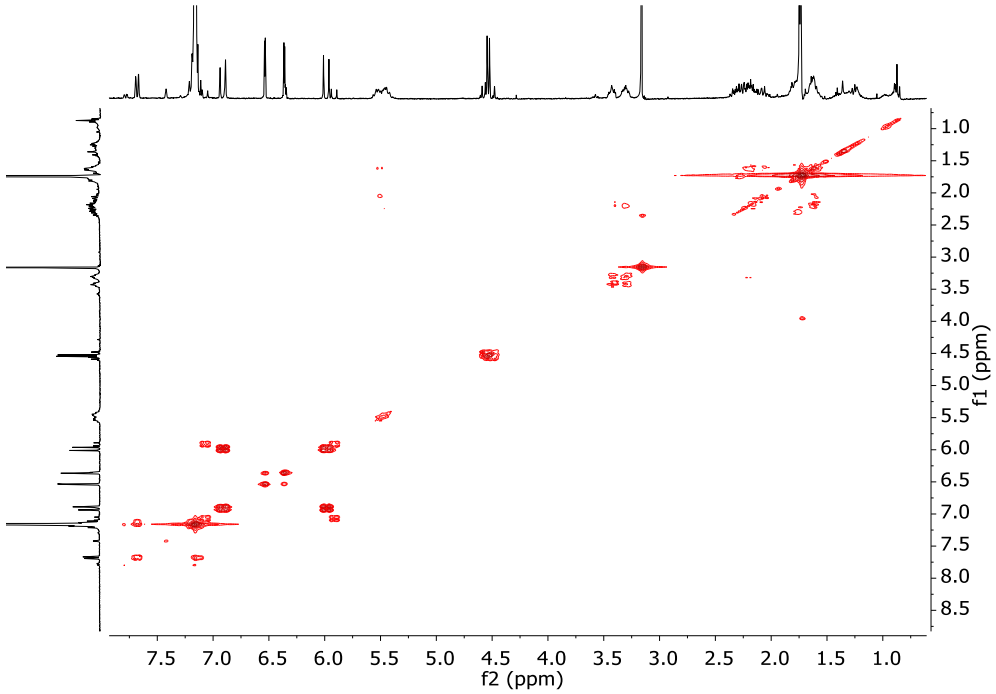

Figure S2. ^{1}H-^{1}H COSY (C_6D_6) of [RhBr(cod)(κ*C*-^{t}BuImCH$_2$PyCH$_2$OMe)] (**2**).

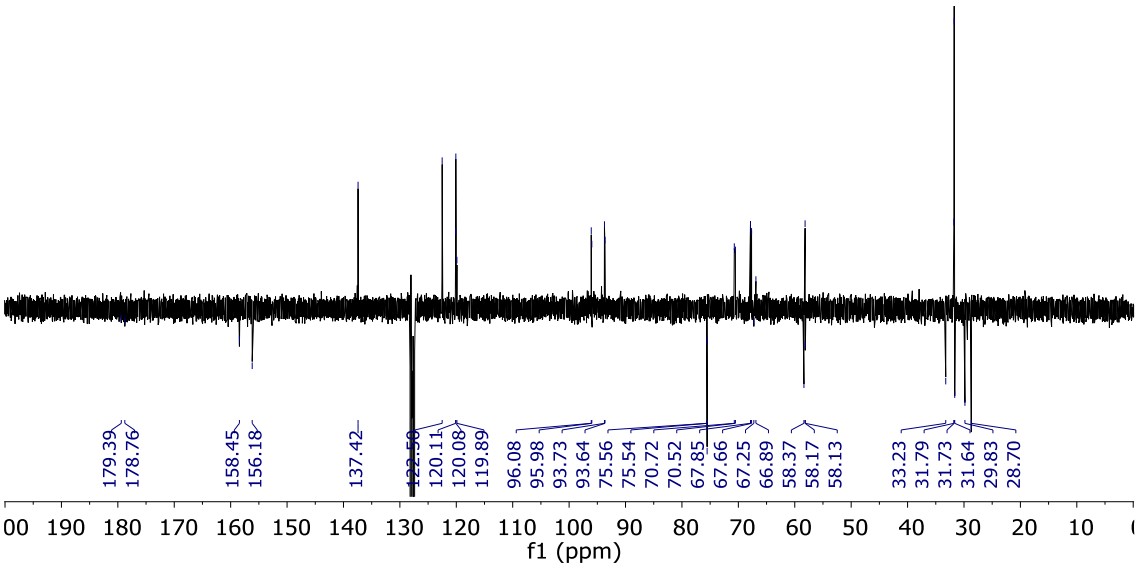

Figure S3. $^{13}C\{^{1}H\}$ NMR (C_6D_6) APT of [RhBr(cod)(κ*C*-^{t}BuImCH$_2$PyCH$_2$OMe)] (**2**).

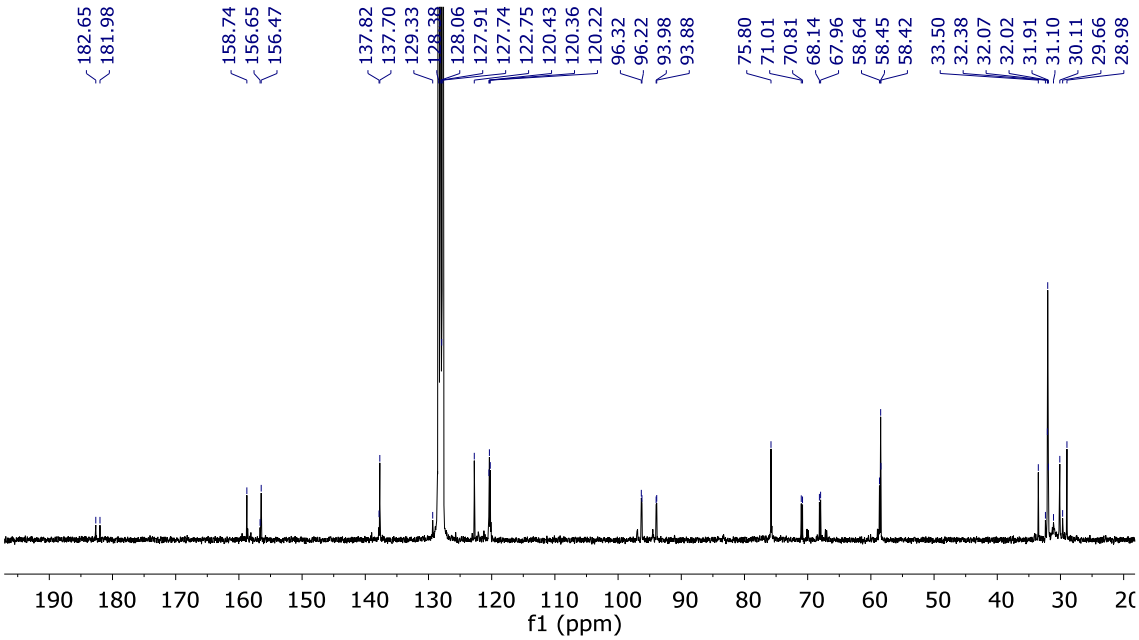

Figure S4. $^{13}C\{^{1}H\}$ NMR (C_6D_6) of [RhBr(cod)(κ*C*-^{t}BuImCH$_2$PyCH$_2$OMe)] (**2**).

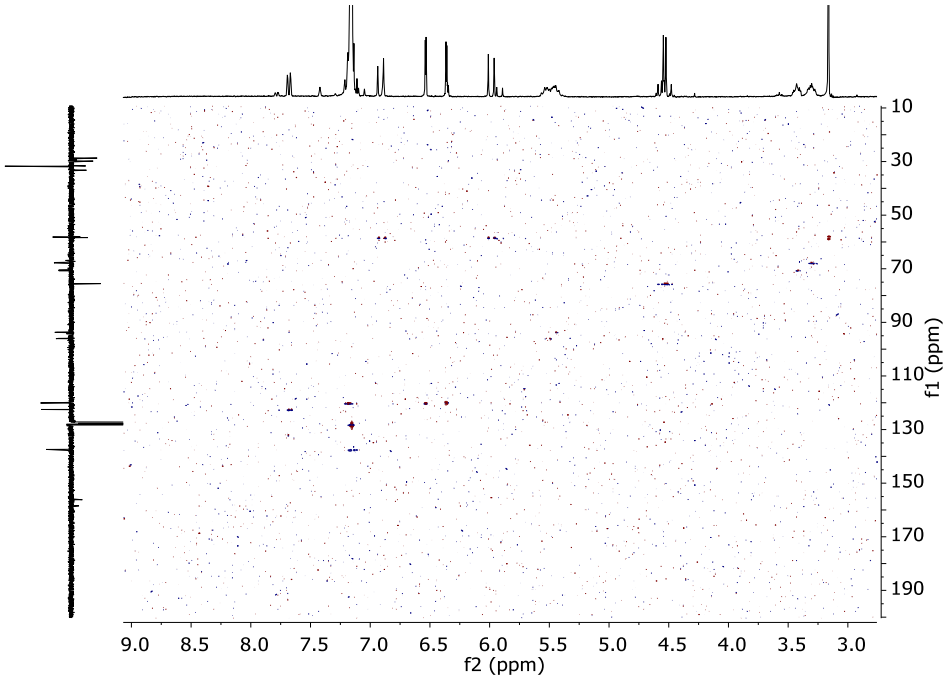

Figure S5. ^{1}H-^{13}C HSQC (C_6D_6) of [RhBr(cod)(κ*C*-^{t}BuImCH$_2$PyCH$_2$OMe)] (**2**).

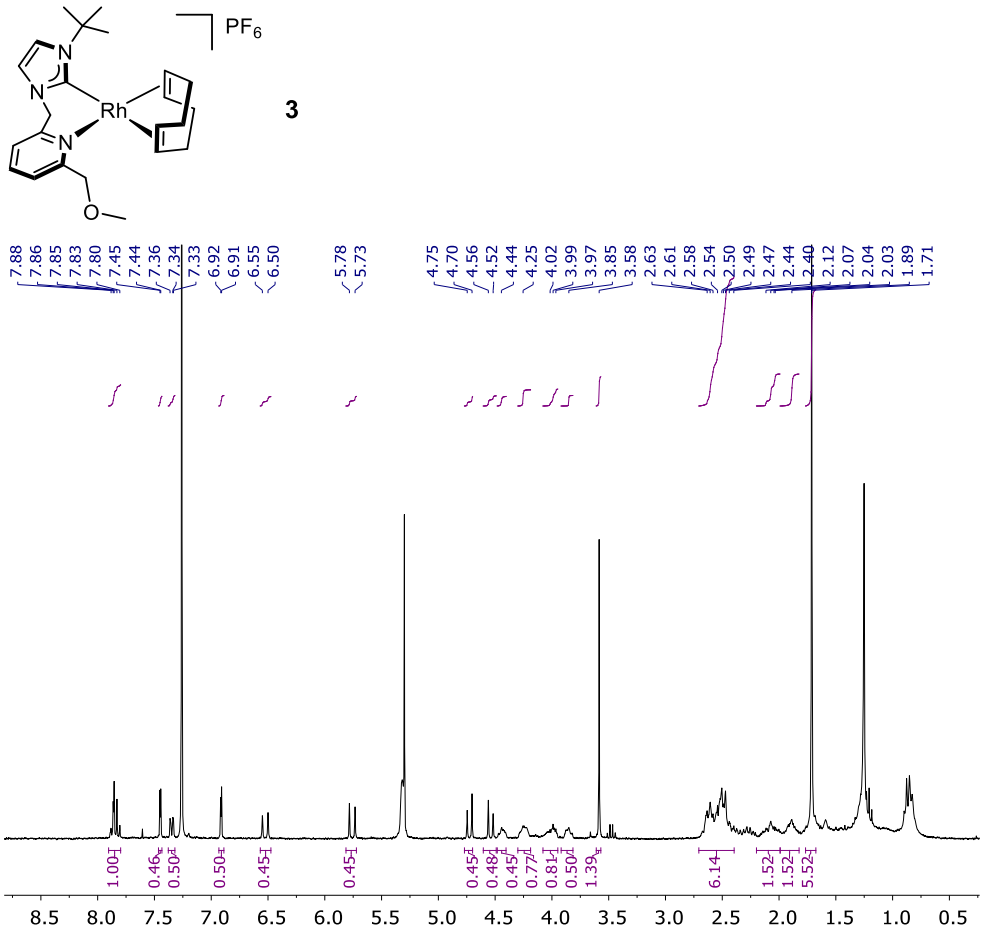

Figure S6. ^{1}H NMR ($CDCl_3$) spectrum of [Rh(cod)(κ^{2}*C*,*N*-^{t}BuImCH$_2$PyCH$_2$OMe)]PF$_6$ (**3**).

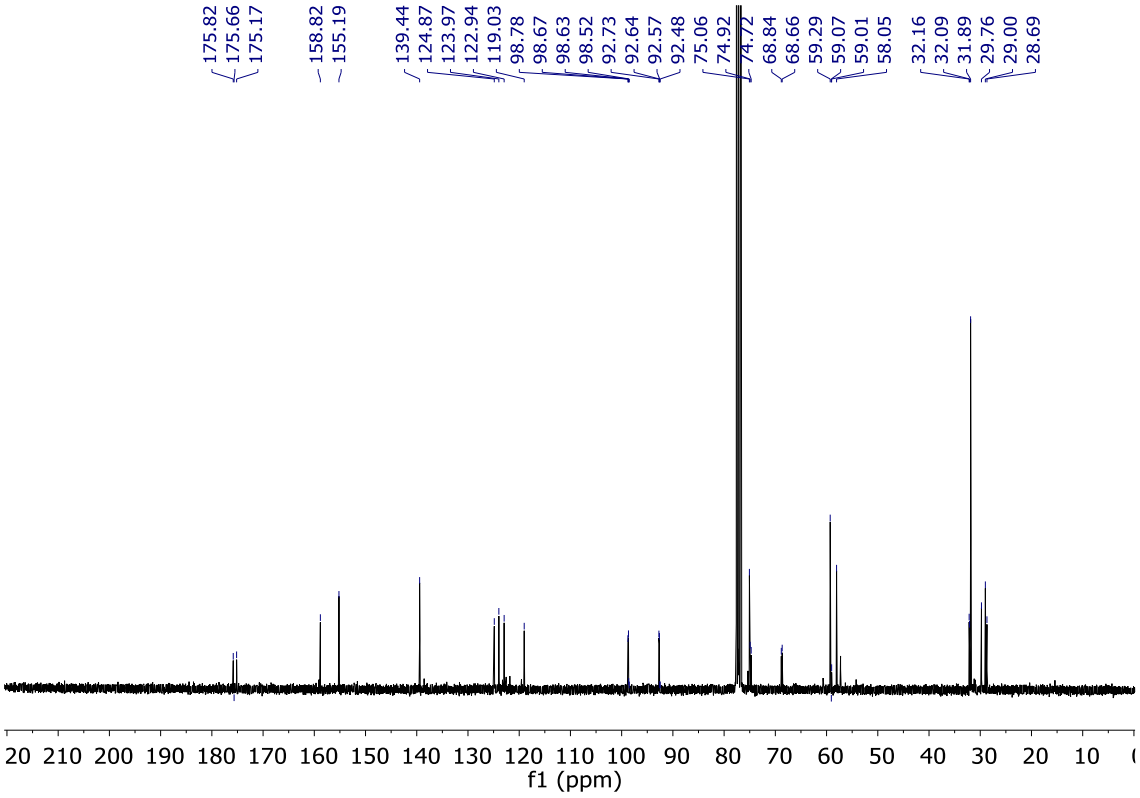

Figure S7. $^{13}C\{^{1}H\}$ NMR (C_6D_6) of [Rh(cod)(κ^2*C*,*N*-^{t}BuImCH$_2$PyCH$_2$OMe)]PF$_6$ (**3**).

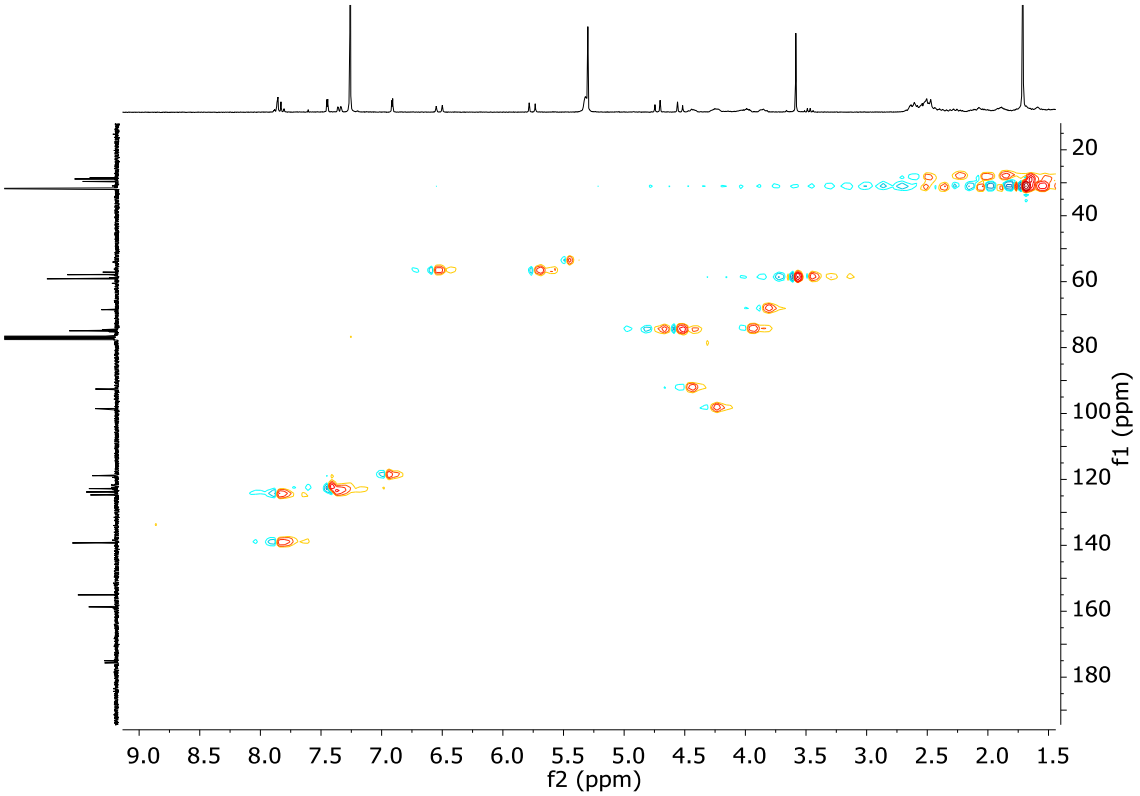

Figure S8. ^{1}H-^{13}C HSQC (C_6D_6) of [Rh(cod)(κ^2*C*,*N*-^{t}BuImCH$_2$PyCH$_2$OMe)]PF$_6$ (**3**).

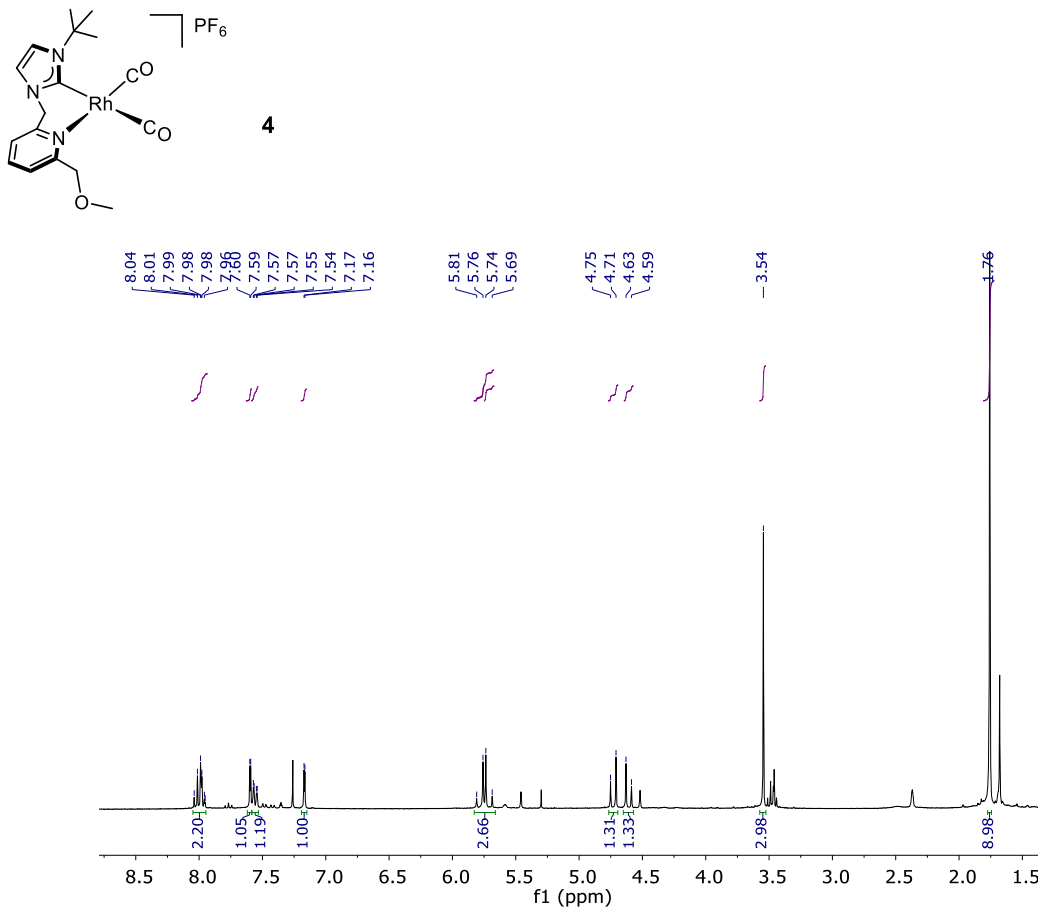

Figure S9. ^{1}H NMR ($CDCl_3$) spectrum of $[Rh(CO)_2(\kappa^2C,N\text{-}^{t}BuImCH_2PyCH_2OMe)]PF_6$ (**4**).

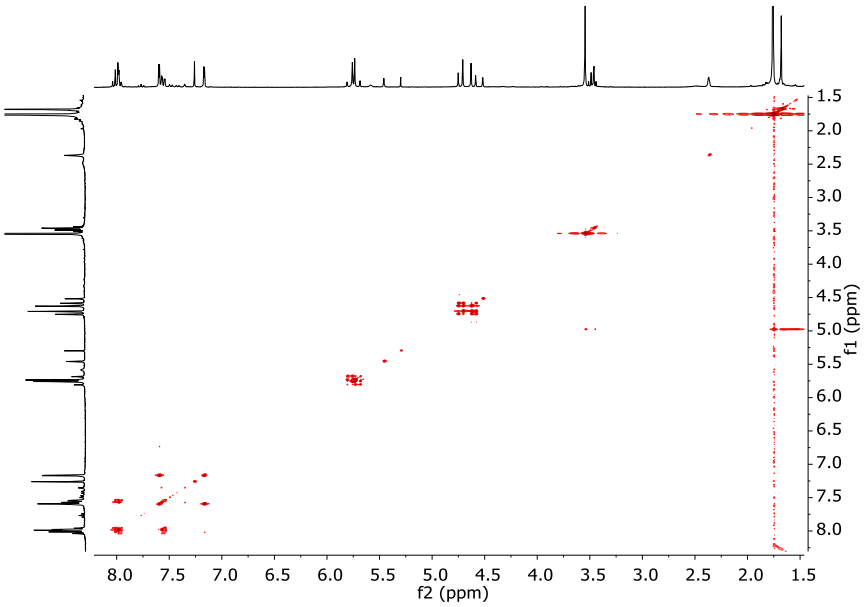

Figure S10. ^{1}H-^{1}H COSY NMR ($CDCl_3$) of $[Rh(CO)_2(\kappa^2C,N\text{-}^{t}BuImCH_2PyCH_2OMe)]PF_6$ (**4**).

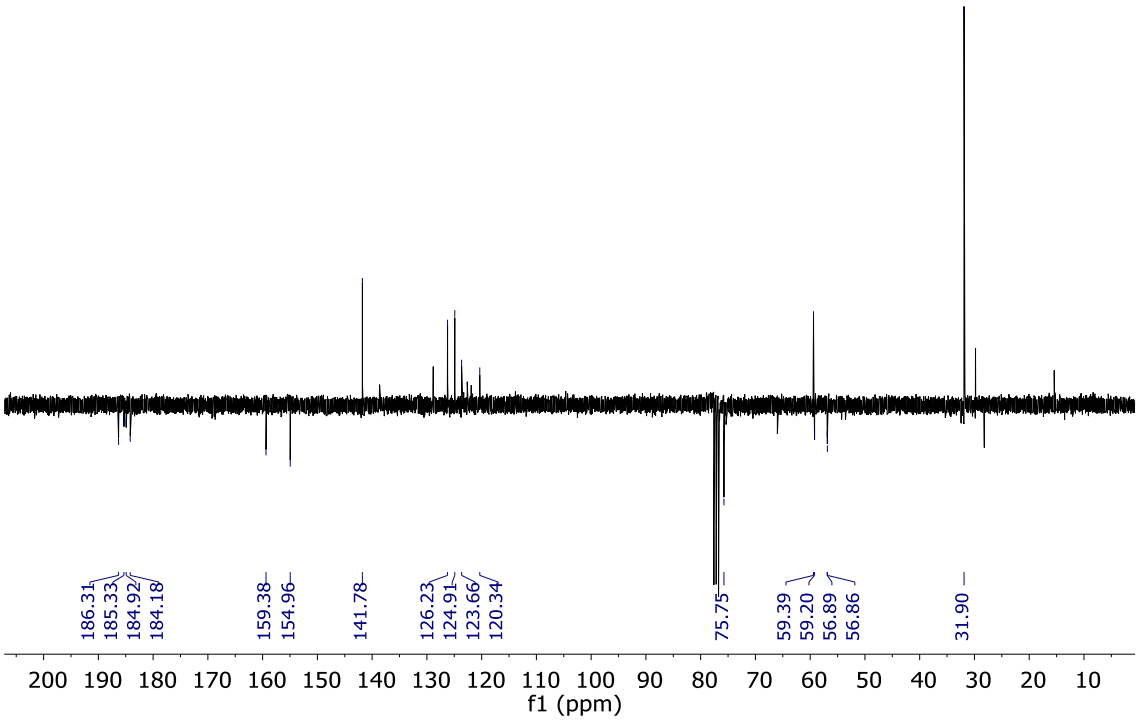

Figure S11. $^{13}C\{^{1}H\}$-APT NMR ($CDCl_3$) spectrum of $[Rh(CO)_2(\kappa^2 C,N\text{-}^{t}BuImCH_2PyCH_2OMe)]PF_6$ (**4**).

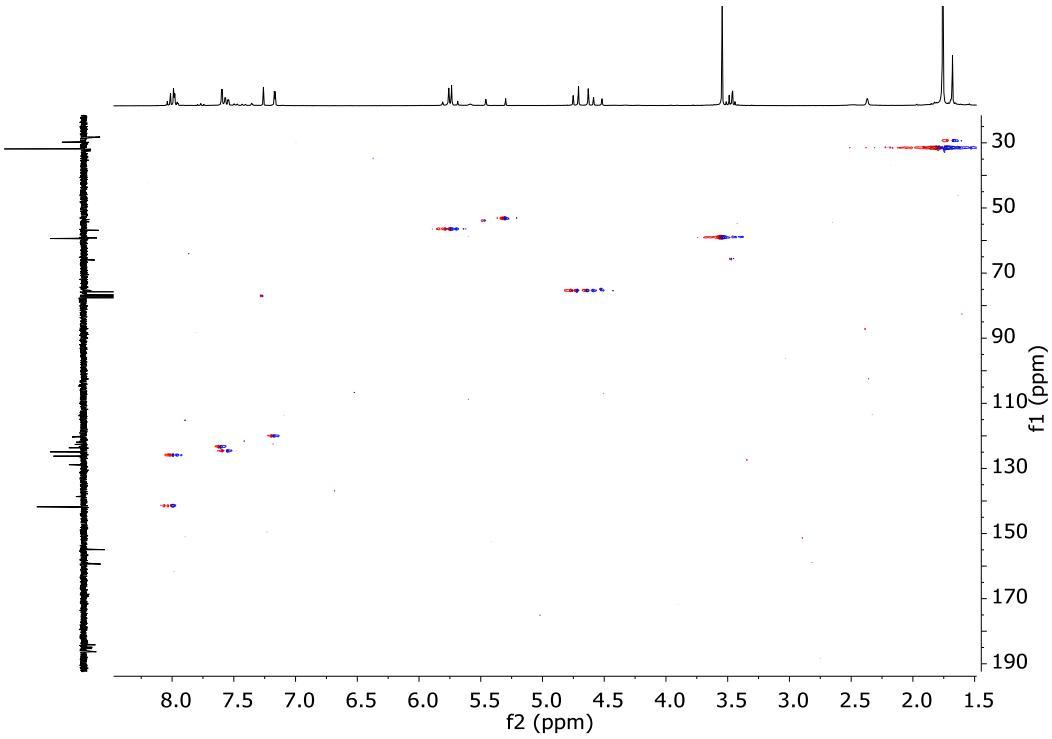

Figure S12. $^{1}H\text{-}^{13}C$ HSQC NMR ($CDCl_3$) of $[Rh(CO)_2(\kappa^2 C,N\text{-}^{t}BuImCH_2PyCH_2OMe)]PF_6$ (**4**).

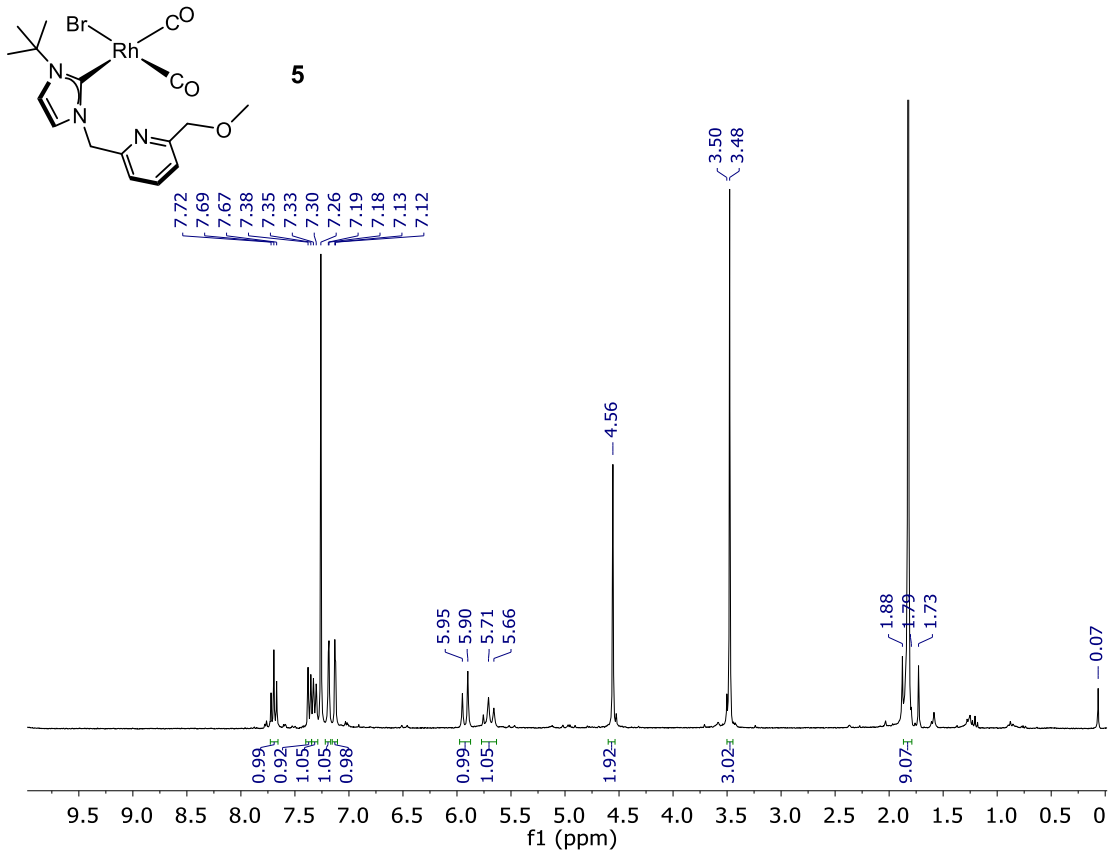

Figure S13. ^{1}H NMR ($CDCl_3$) spectrum of [RhBr(CO)$_2$(κ*C*-^{t}BuImCH$_2$PyCH$_2$OMe)] (**5**).

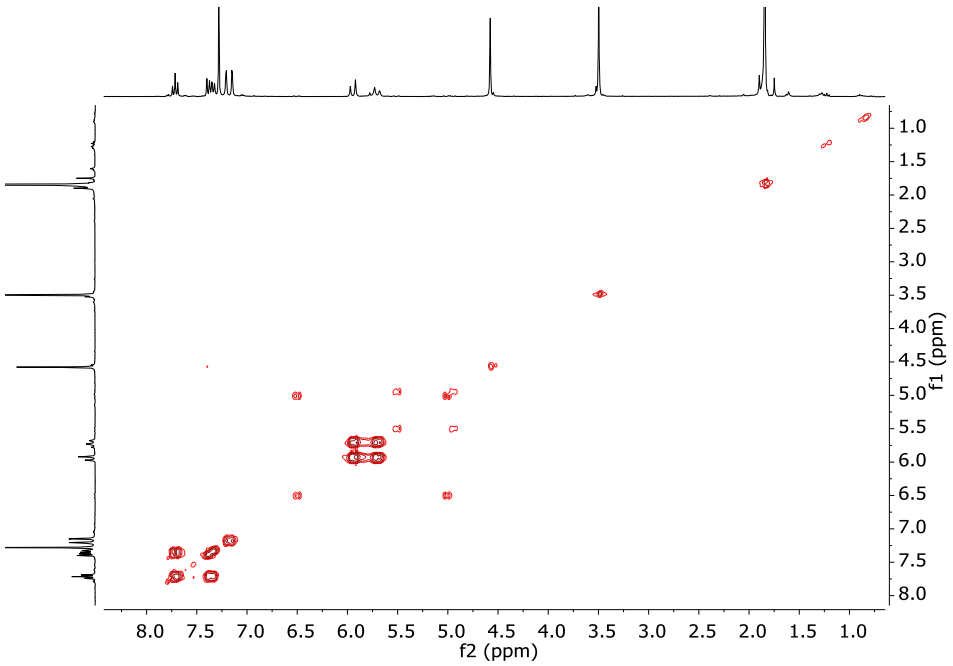

Figure S14. ^{1}H-^{1}H COSY NMR ($CDCl_3$) of [RhBr(CO)$_2$(κ*C*-^{t}BuImCH$_2$PyCH$_2$OMe)] (**5**).

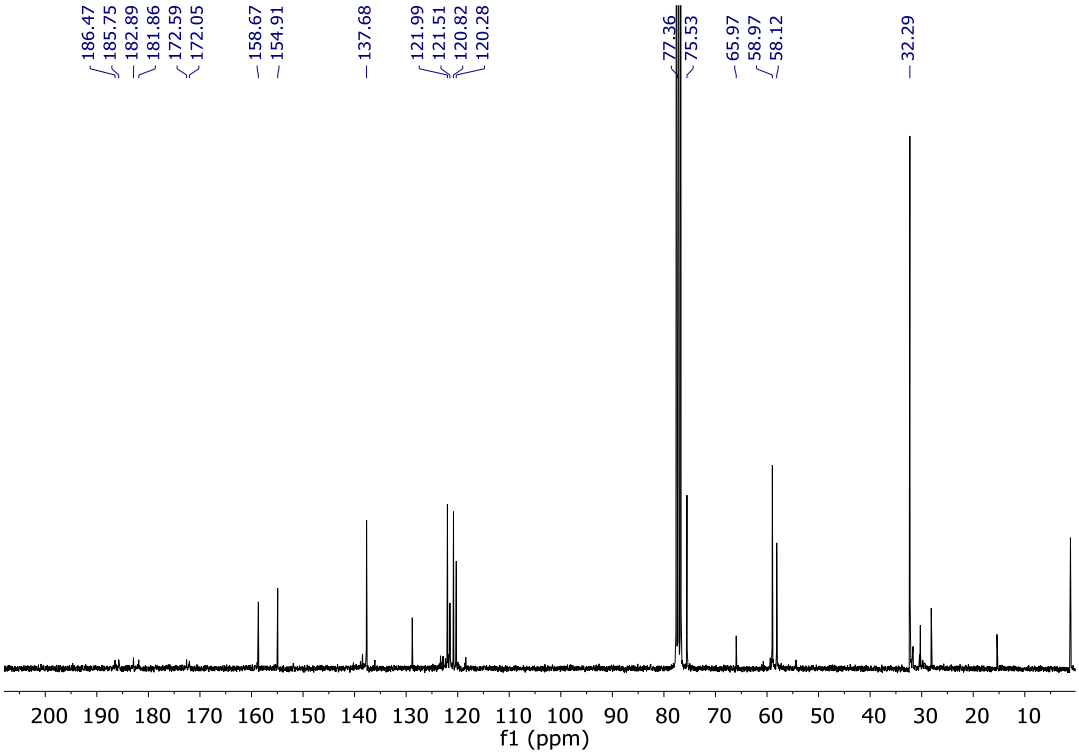

Figure S15. $^{13}C\{^{1}H\}$ NMR ($CDCl_3$) of [RhBr(CO)$_2$(κ*C*-^{t}BuImCH$_2$PyCH$_2$OMe)] (**5**).

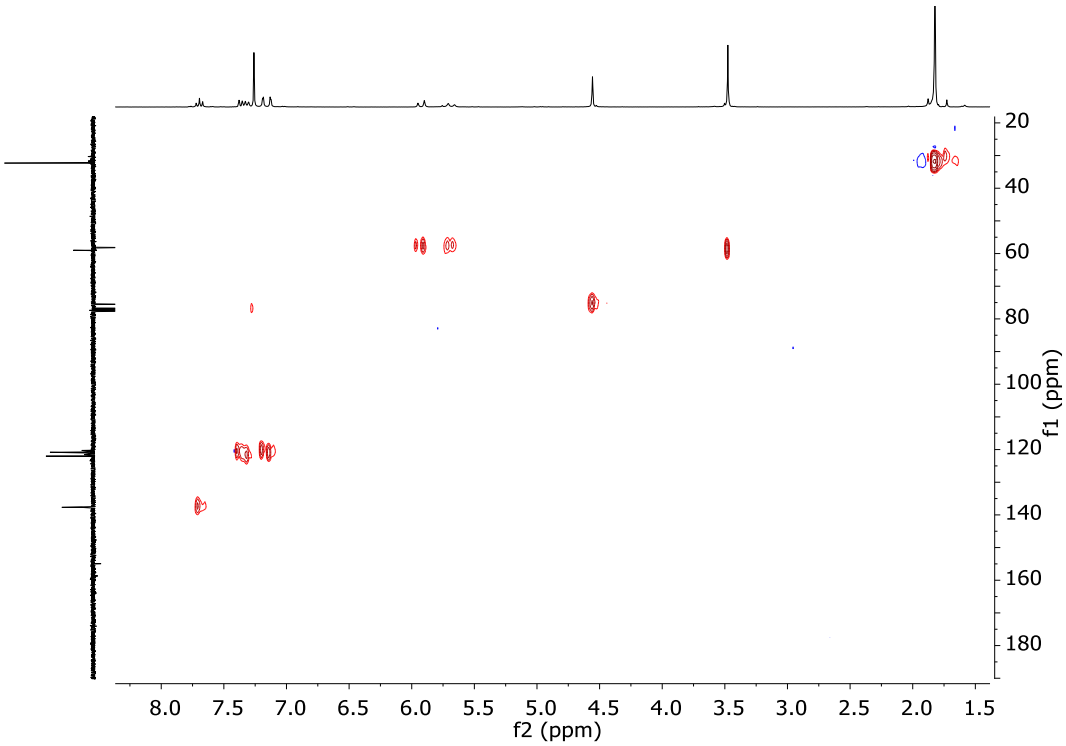

Figure S16. ^{1}H-^{13}C HSQC NMR ($CDCl_3$) of [RhBr(CO)$_2$(κ*C*-^{t}BuImCH$_2$PyCH$_2$OMe)] (**5**).

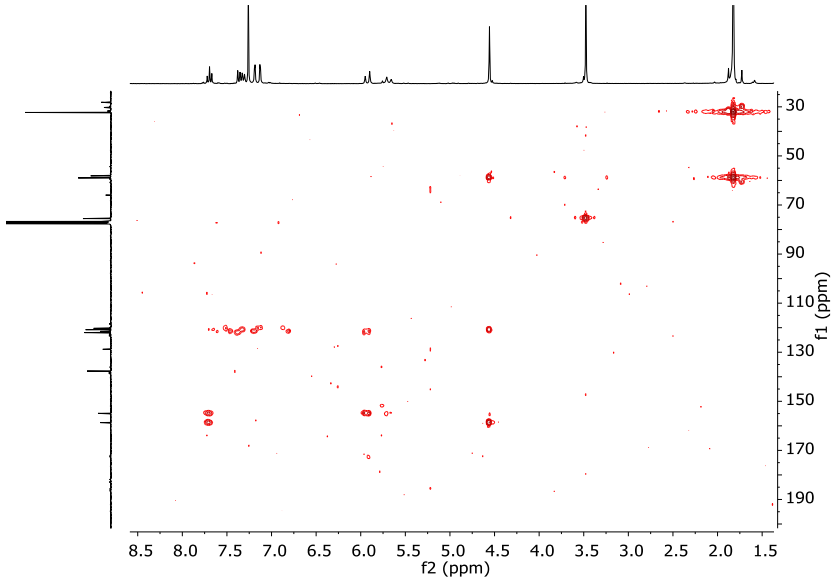

Figure S17. ^{1}H-^{13}C HMBC NMR ($CDCl_3$) of [RhBr(CO)$_2$(κ*C*-^{t}BuImCH$_2$PyCH$_2$OMe)] (**5**).

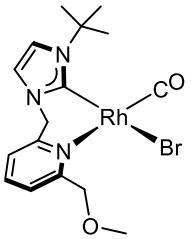

6

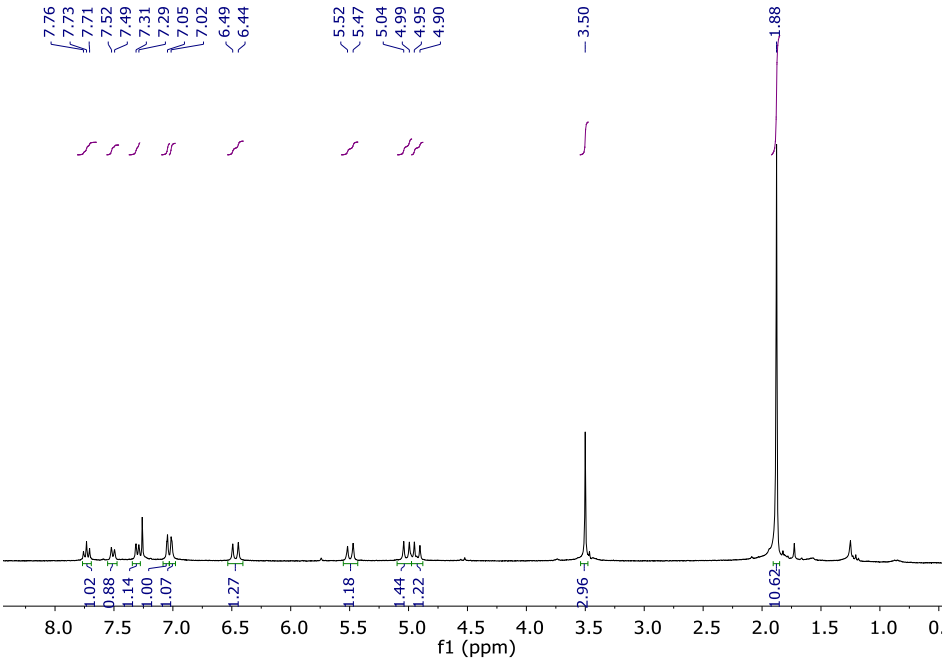

Figure S18. ^{1}H NMR ($CDCl_3$) spectrum of [RhBr(CO)(κ^{2}*C*,*N*-^{t}BuImCH$_2$PyCH$_2$OMe)] (**6**).

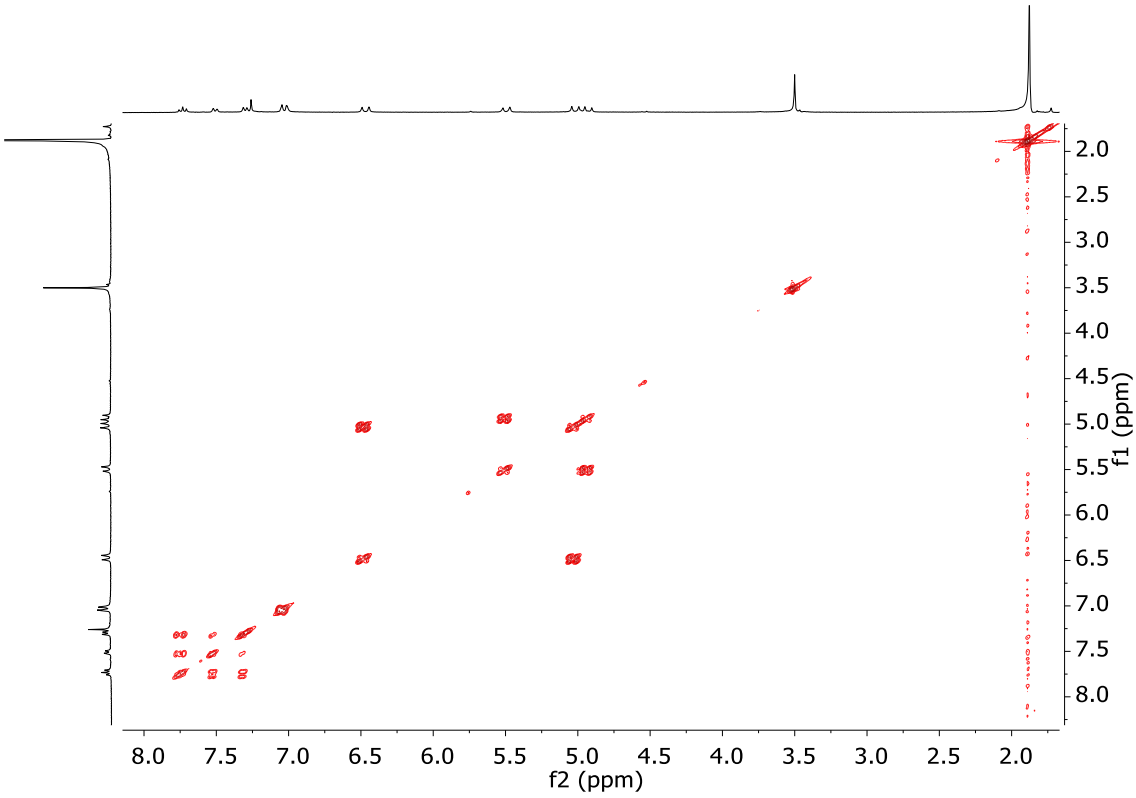

Figure S19. ^{1}H-^{1}H COSY NMR ($CDCl_3$) of [RhBr(CO)(κ^{2}*C,N* -^{t}BuImCH$_2$PyCH$_2$OMe)] (**6**).

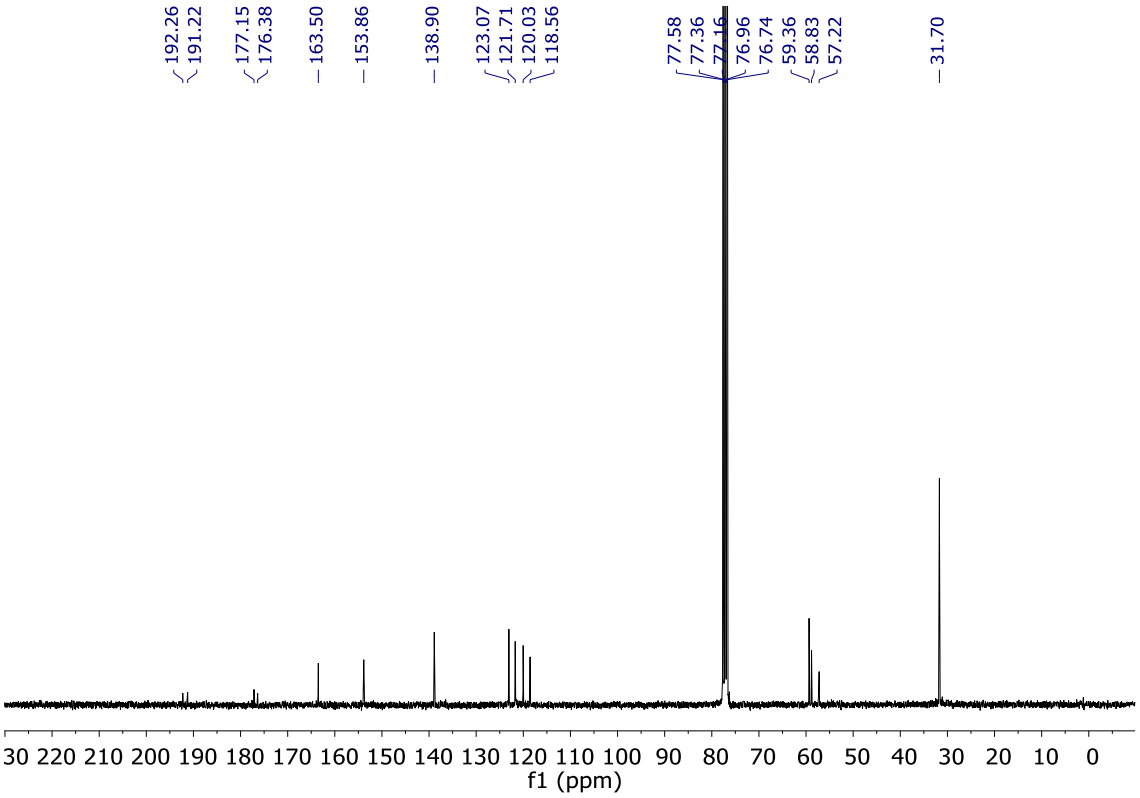

Figure S20. ^{13}C{^{1}H} NMR ($CDCl_3$) of [RhBr(CO)(κ^{2}*C,N* -^{t}BuImCH$_2$PyCH$_2$OMe)] (**6**).

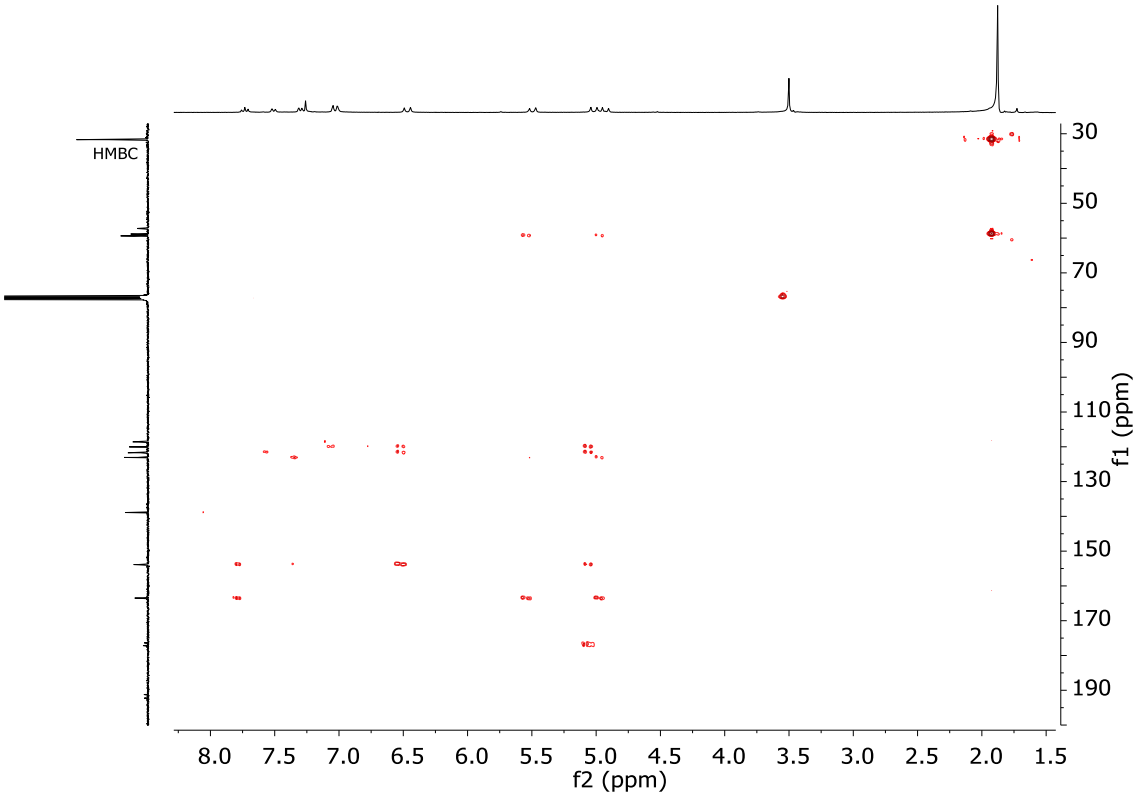

Figure S21. ^{1}H-^{13}C HMBC NMR ($CDCl_3$) of [RhBr(CO)(κ^{2}*C*,*N*-^{t}BuImCH$_2$PyCH$_2$OMe)] (**6**).

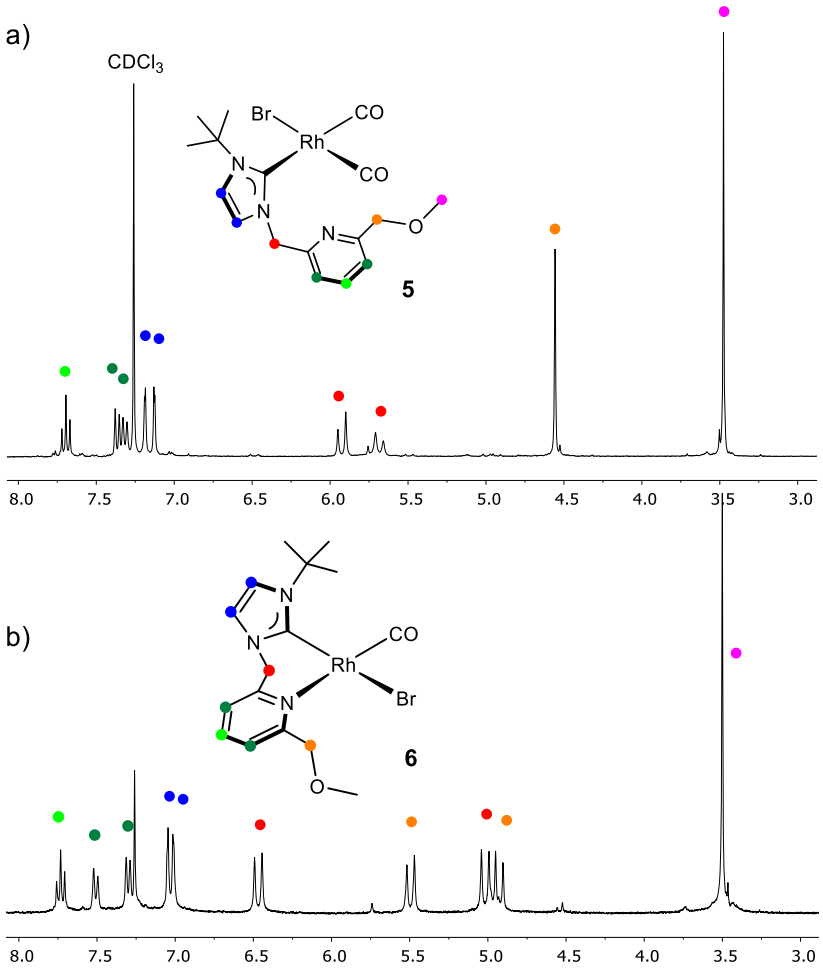

Figure S22. Comparison of the ^{1}H NMR spectra of complexes **5** and **6** in $CDCl_3$.

2.- ATR-IR spectra of carbonyl compounds 4-6.

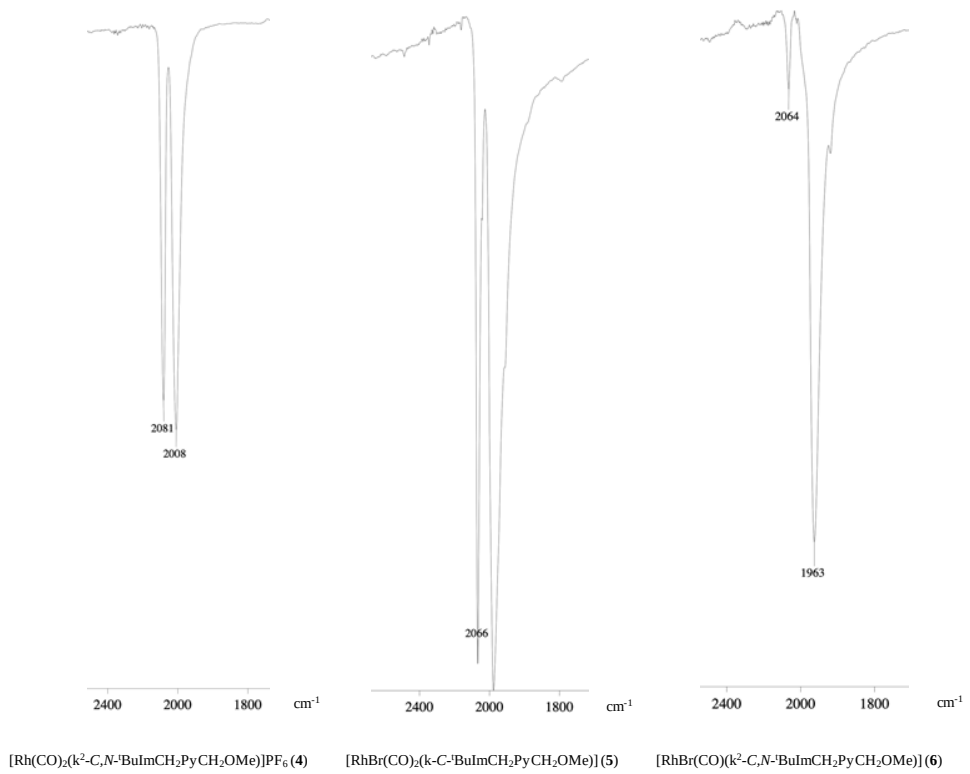

Figure S23. Terminal carbonyl region of the ATR-IR spectra of compounds **4-6** (ν(CO) in cm $^{-1}$).

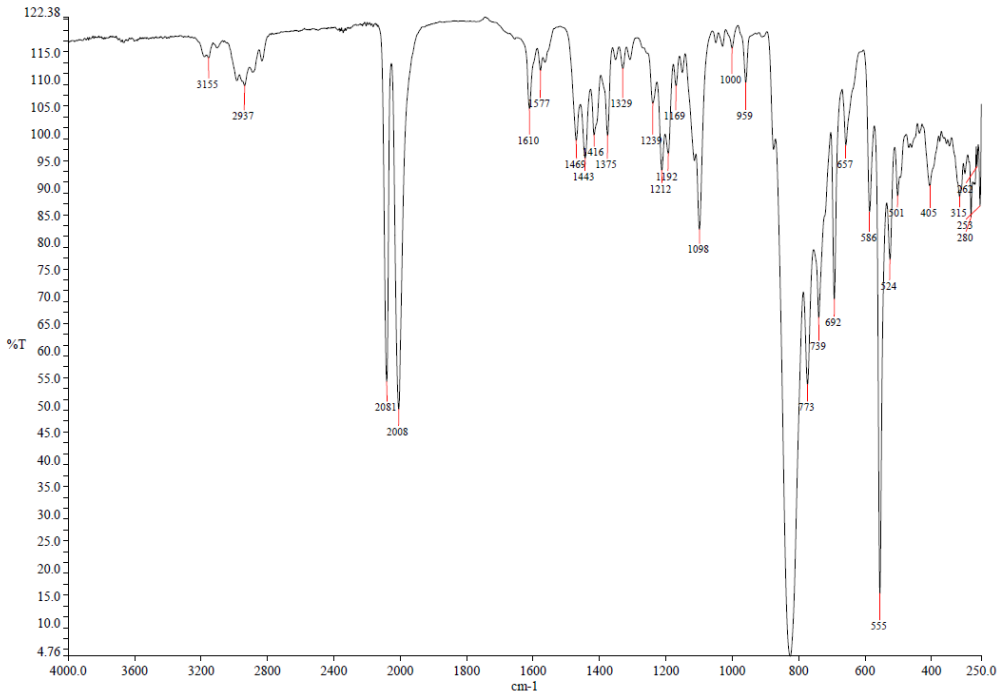

Figure S24. ATR-IR spectrum of [Rh(CO)$_2$(κ^2*C*,*N*-^{t}BuImCH$_2$PyCH$_2$OMe)]PF$_6$ (**4**).

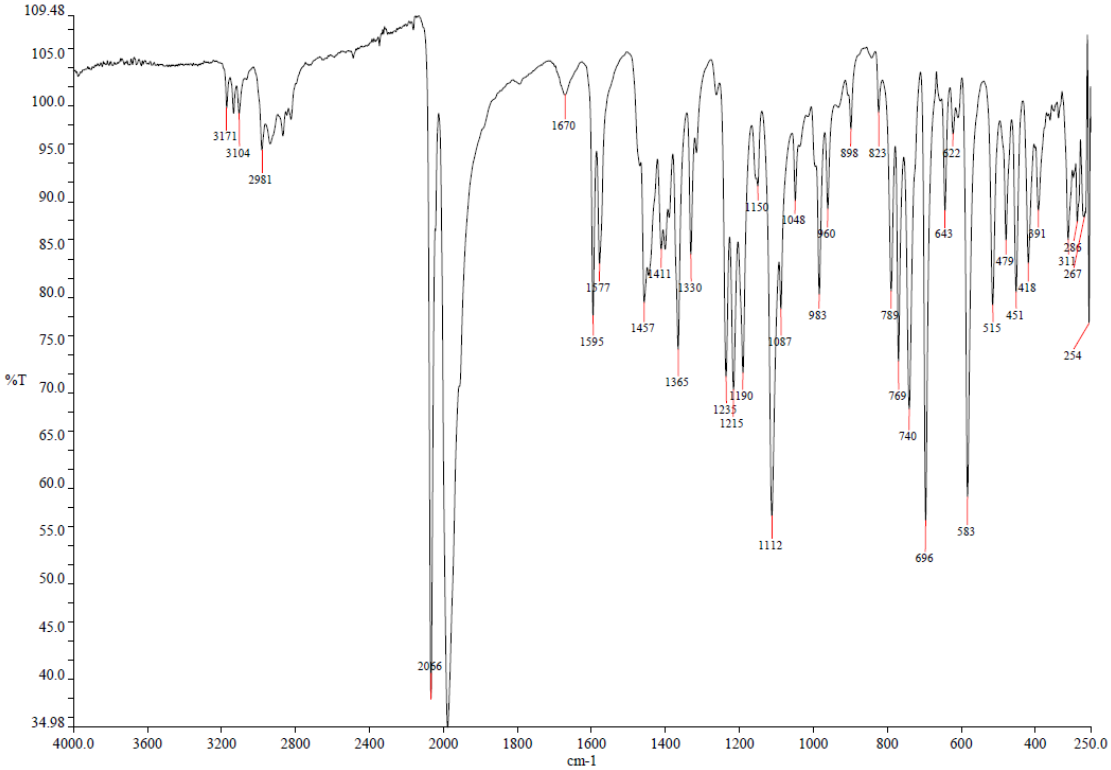

Figure S25. ATR-IR spectrum of [RhBr(CO)$_2$(κ*C*-^{t}BuImCH$_2$PyCH$_2$OMe)] (**5**).

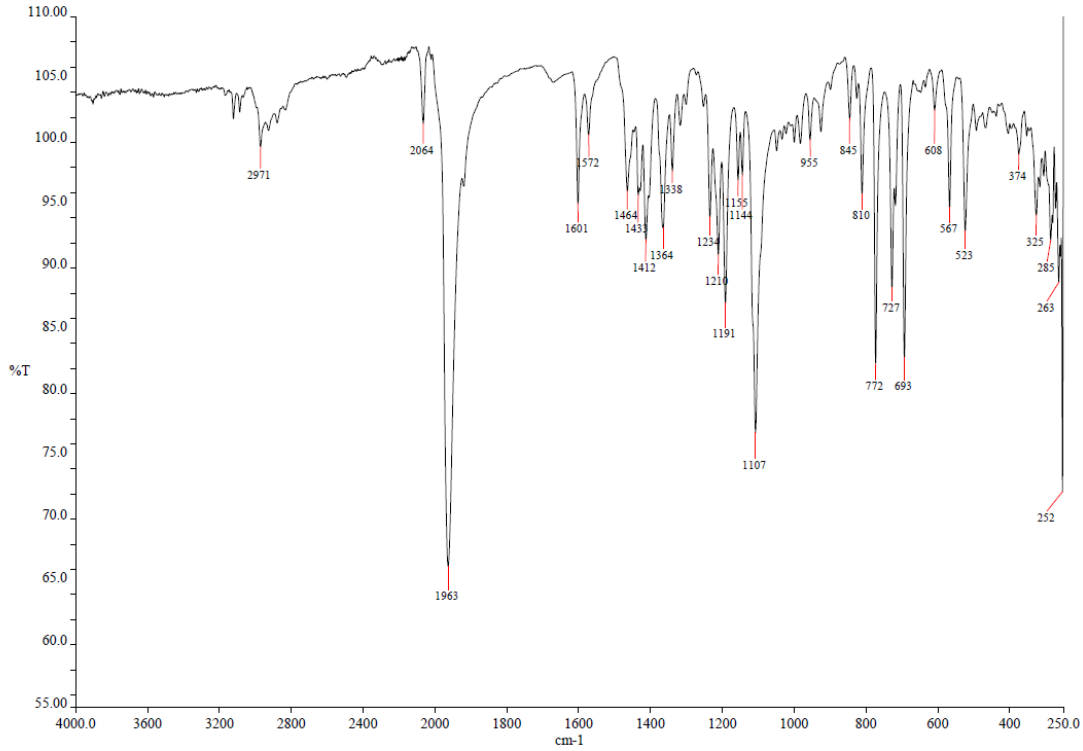

Figure S26. ATR-IR spectrum of [RhBr(CO)(κ^2*C*,*N*-^{t}BuImCH$_2$PyCH$_2$OMe)] (**6**).

3.- Hydrosilylation of phenylacetylene derivatives with $HSiMe_2Ph$ catalyzed by 6.

a)

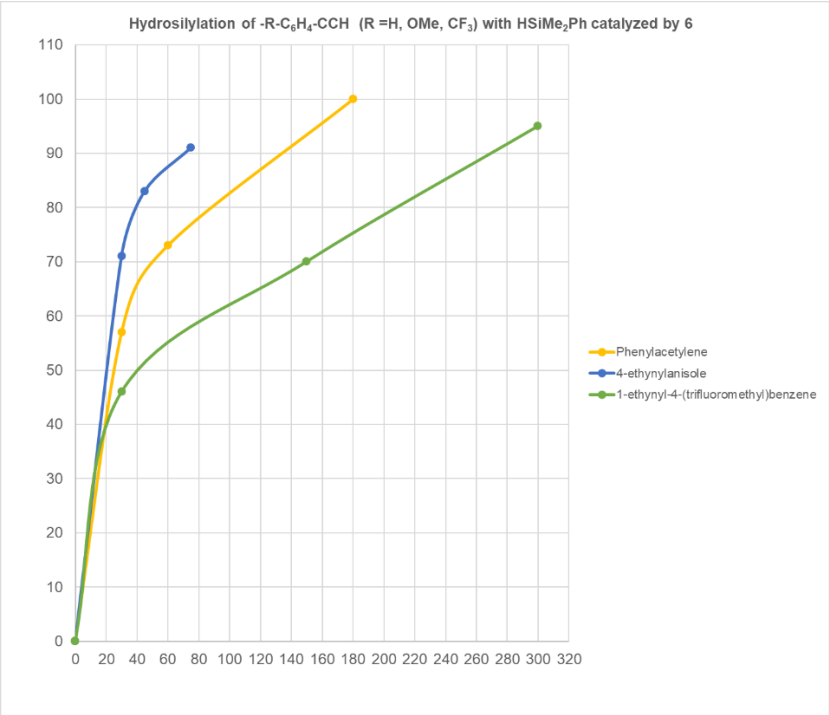

b)

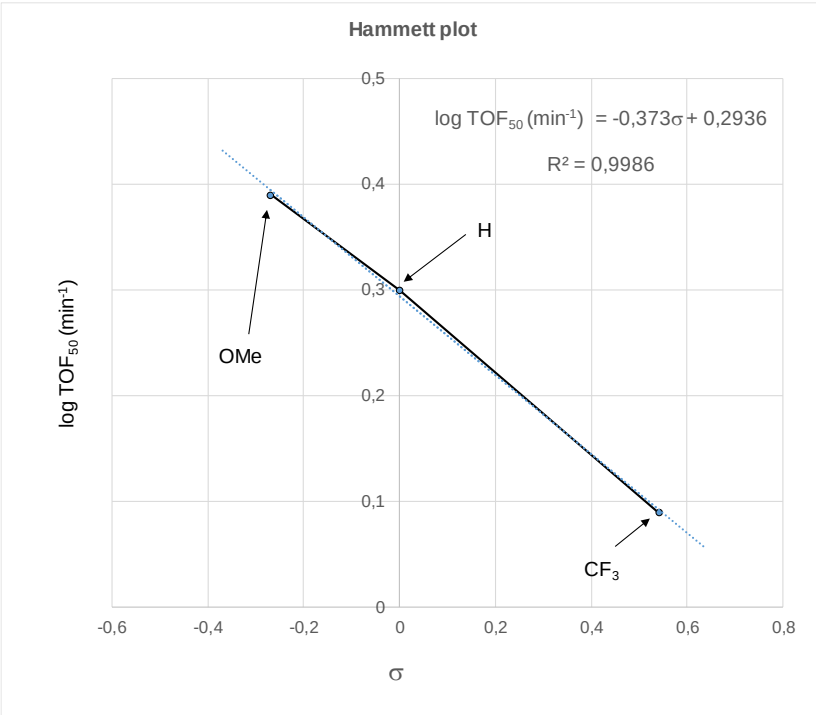

Figure S27. a) Reaction profile obtained from ^{1}H-NMR data for the hydrosilylation of phenylacetylene derivatives 4-R-C_6H_4–C≡CH (R = H, yellow; MeO, blue; and CF_3, green) with $HSiMe_2Ph$ (1:1), in $CDCl_3$ (0.5 mL) at 333 K catalyzed by **6**. b) Hammett plot.

4.- Hydrosilylation of terminal alkynes with $HSiMe_2Ph$ catalyzed by 6 at different reaction times.[a]

Table S1. Hydrosilylation of terminal alkynes catalyzed by **6**.

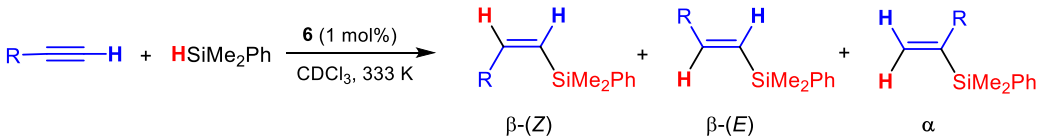

	Silane	Alkyne	Time	Conversion (%)[b]	Selectividad (%)[b]		
					β-(*Z*)	β-(*E*)	α
1			10’	57	92	5	3
2	$HSiMe_2Ph$	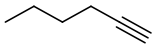	20’	90	92	5	3
3			30’	100	90	6	4
4		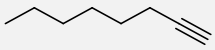	15’	95	87	7	6
5			20’	100	88	6	6
6			30’	28	2	67	31
7			6 h	92	5	55	40
8[c]		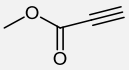	30’	64	-	40	47
9[c]			3 h	100	-	44	47
10		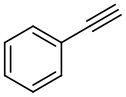	30’	57	67	21	12
11			2 h	100	67	21	12
12		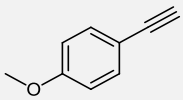	30’	71	74	17	9
13			75’	91	68	24	8
14[d]		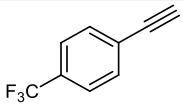	30’	46	42	35	23
15[d]			5 h	95	57	26	17
16		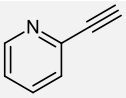	24 h	23	43	49	8
17		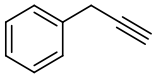	1h 30’	33	74	15	11
18			6 h	96	77	15	8
19	$HSiMePh_2$	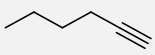	10’	49	100	-	-
20			30’	95	100	-	-
21	$HSiPh_3$	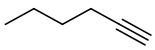	6 h	30	100	-	-
22			24 h	87	100	-	-
23	$HSiEt_3$	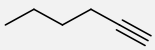	30’	44	86	7	7
24			1 h	65	89	6	5

25			90’	96	89	6	5
26	$HSiMe_2Et$	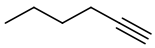	30’	98	89	7	4
27	$HSiMePh_2$		3 h	26	10	40	50
28			24 h	100	8	40	52
29		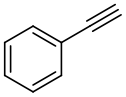	3 h	22	29	42	29
30			7 h	35	28	43	28
31			24 h	59	29	43	28
32		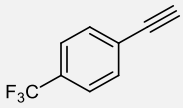	3 h	24	16	55	29
33			7 h	67	45	33	22
34			24 h	59	22	51	27
35		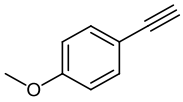	3 h	33	44	34	22
36			7 h	37	19	51	31
37			24 h	100	42	39	19

[a] Reaction conditions: alkyne (0.11 mmol), $HSiMe_2Ph$ (0.11 mmol) and **6** (0.0011 mmol, 1.0 mol%), in $CDCl_3$ (0.5 mL) at 333 K. [$HSiMe_2Ph$] = [1-alkyne] ≈ 0.22 M. [b] Conversion, based on $HSiR_3$, and selectivity determined by ^1H RMN using anisole as internal standard. [c] 13% and 9% of methylacrilate. [d] Traces of 1-trifluoromethyl-4-vinylbenzene were observed.

5.- Isomerization β-(*Z*)→β-(*E*) in the hydrosilylation of PhC≡CH with $HSiMe_2Ph$ catalyzed by 6.

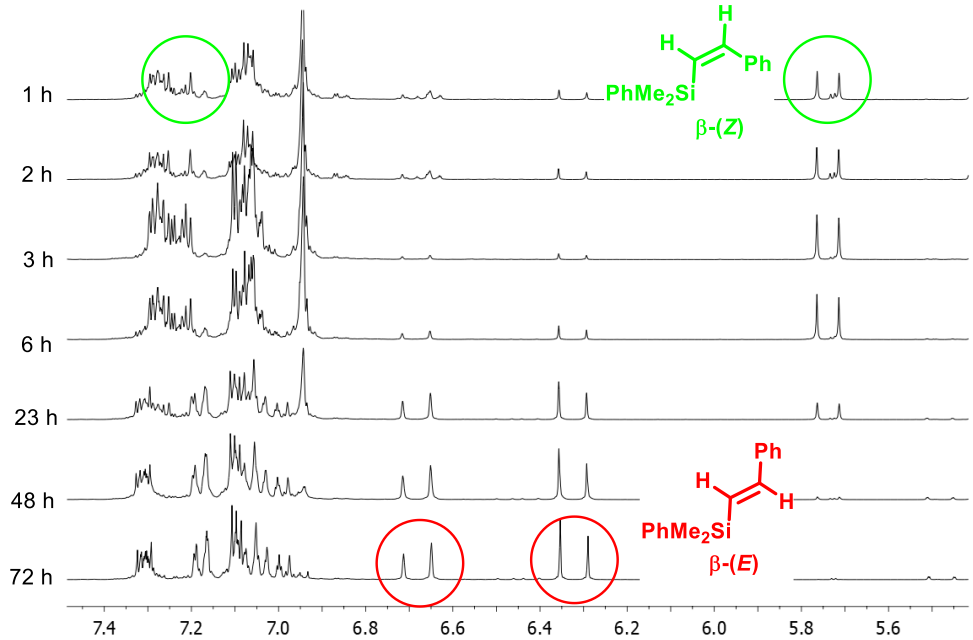

Figure S28. ^{1}H-NMR ($CDCl_3$) spectra of the hydrosilylation of PhC≡CH with $HSiMe_2Ph$ catalyzed by **6** at long reaction times. Reaction conditions: phenylacetylene (0.11 mmol), $HSiMe_2Ph$ (0.11 mmol) and **6** (0.0011 mmol, 1 mol%) in $CDCl_3$ (0.5 mL) at 333 K.

6.- Reaction of 6 with 20 eq. of $HSi(OEt)_3$

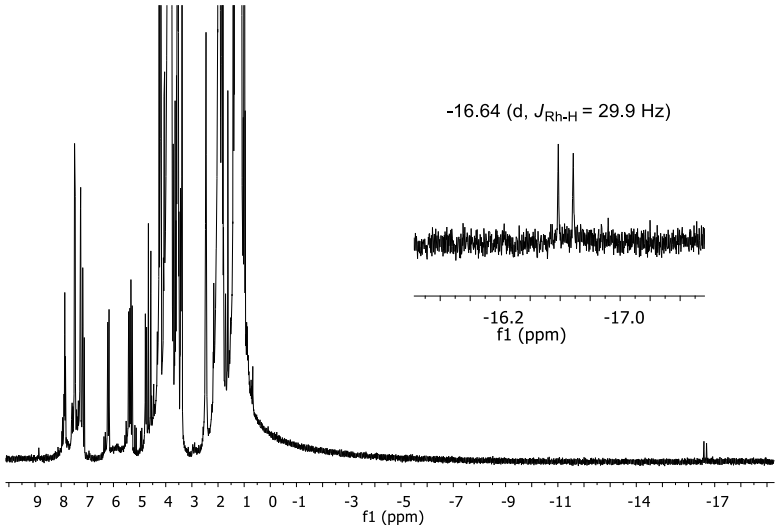

Figure S29. ^{1}H NMR (acetonitrile-d_3, 300K) of the reaction of [RhBr(CO)(k^2-*C*,*N*-^{t}BuImCH$_2$PyCH$_2$OMe)] (**6**) with 20 eq. of $HSi(OEt)_3$ at 333K for 1h.

7.- Determination of activation parameters for the hydrosilylation of 1-hexyne with $HSiMe_2Ph$ catalyzed by 6 in $CDCl_3$.

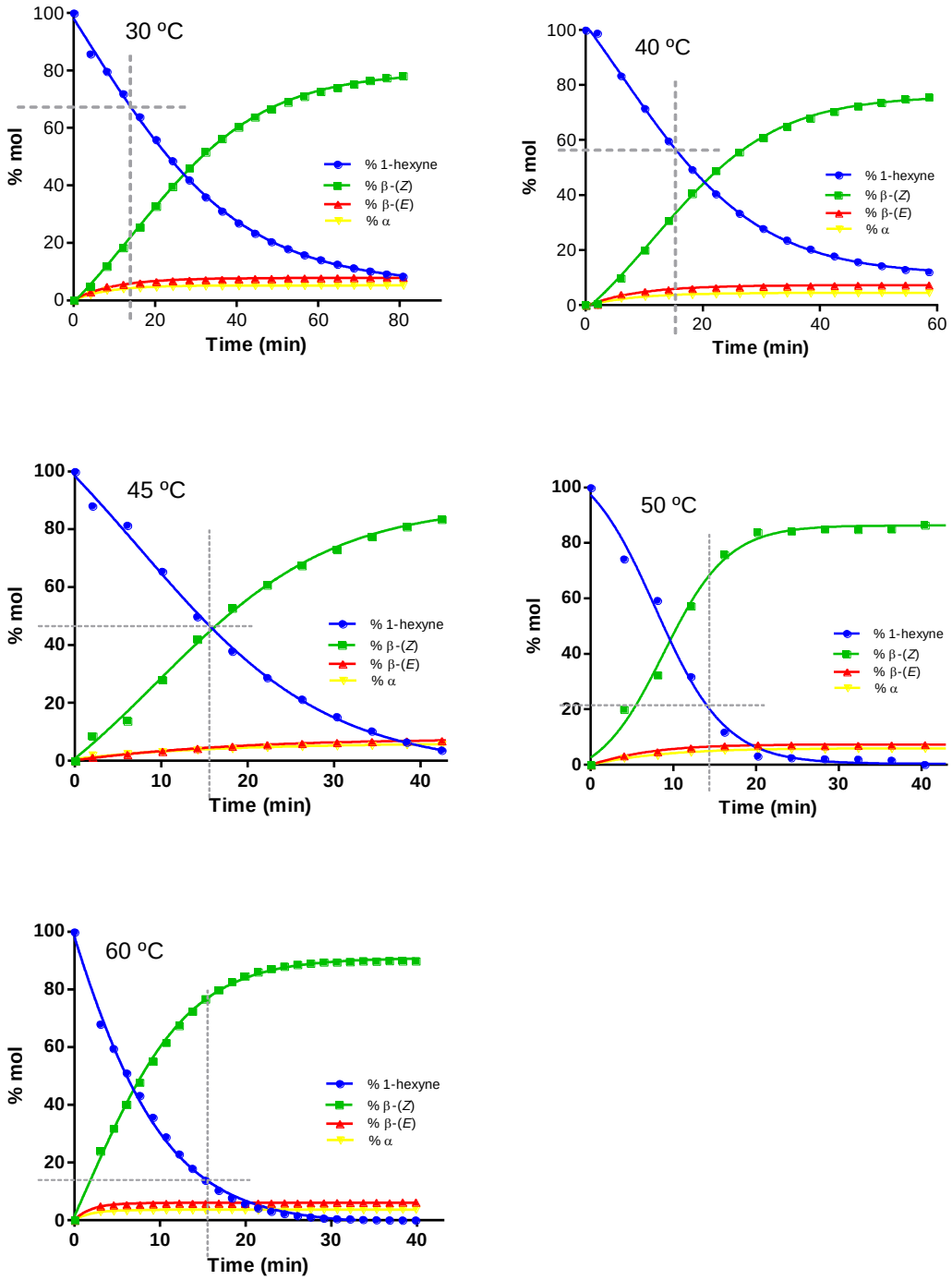

Figure S30. Reaction profiles for the hydrosilylation of 1-hexyne with $HSiMe_2Ph$ monitored by ^1H NMR at the indicated temperature. Reaction conditions: hydrosilane (0.11 mmol), alkyne (0.11 mmol) and **6** (1 mol%) in $CDCl_3$ (0.5 mL).

Table S2. Influence of the temperature in the hydrosilylation of 1-hexyne to β-(*Z*)-hex-1-enyldimethyl(phenyl)silane catalyzed by **6**.[a,b]

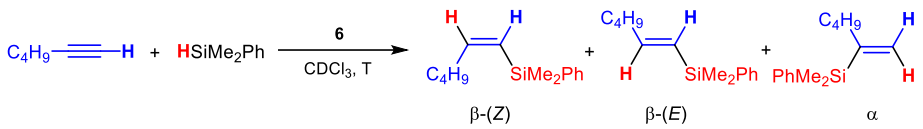

	T (K)	t (min)	Conversion (%)[b]	Selectivity (%)[b]		
				β-(*Z*)	β-(*E*)	α
1	303	15	34	71	17	12
2		81	92	87	8	5
3	313	15	43	77	14	9
4		58	88	86	8	6
5	318	15	53	85	8	7
6		50	100	87	7	6
7	323	15	77	84	9	7
8		44	100	87	7	6
9	333	15	86	89	7	4
10		30	100	90	6	4

[a] Reaction conditions: 1-hexyne (0.10 mmol), $HSiMe_2Ph$ (0.10 mmol) and **6** (0.001 mmol, 1.0 mol%), in $CDCl_3$ (0.5 mL). [b] Conversion, based on $HSiMe_2Ph$, and selectivity determined by ^1H NMR.

The Gibbs free energy barrier ($\Delta G^{\ddagger}$) and the activation parameters, $\Delta H^{\ddagger}$ and $\Delta S^{\ddagger}$, were determined from a linear least squares fit of the temperature dependence of the initial turnover frequency determined at 15 min reaction time, TOF_o (s^{-1}), to the logarithmic form of the Eyring equation.

Free energy equation:

$$\Delta G^{\ddagger} = \Delta H^{\ddagger} - T\Delta S^{\ddagger}$$

Erying equation:

$$k = K\frac{k_b T}{h}e^{\frac{-\Delta G^{\ddagger}}{RT}} \qquad K = 1$$

$$\ln\left(\frac{k}{T}\right) = -\frac{\Delta H^{\ddagger}}{R}\cdot\frac{1}{T} + \ln\left(\frac{k_b}{h}\right) + \frac{\Delta S^{\ddagger}}{R}$$

where T is temperature in Kelvin, k_b is the Boltzmann's constant and h is Planck's constant.

T	1/T	k (s^{-1})	ln (k/T)
303	0,003299	0,026667	-9,338074
313	0,003193	0,036667	-9,052090
318	0,003143	0,050000	-8,757784
323	0,003095	0,072222	-8,405660
333	0,003002	0,085556	-8,266732

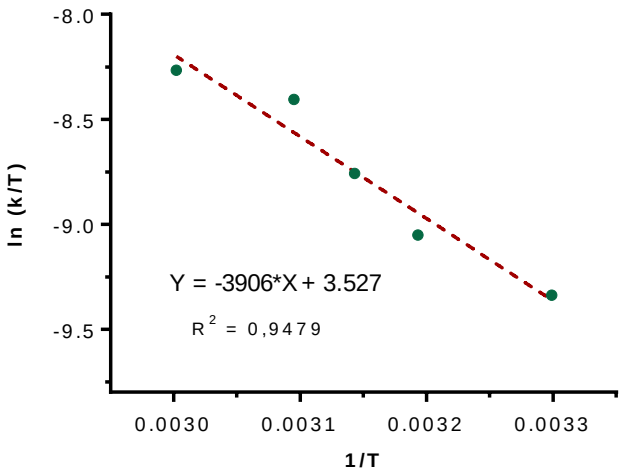

Figure S31. Eyring plot for the hydrosilylation of 1-hexyne with $HSiMe_2Ph$ catalyzed by **6** in $CDCl_3$. The line represents the least squares fit to the data point.

Slope: -3906 Intercept: 3.53 R^2: 0.9479;

ΔH‡ (kcal mol^{-1}): 7.8 ± 1.0; **ΔS**‡ (J/K·mol): -40.2 ± 3.3

ΔG‡ (kJ mol^{-1}): 19.8 ± 2.0 at 298 K

8.- Scan of the Si⋯O coordinates en route from II → III.

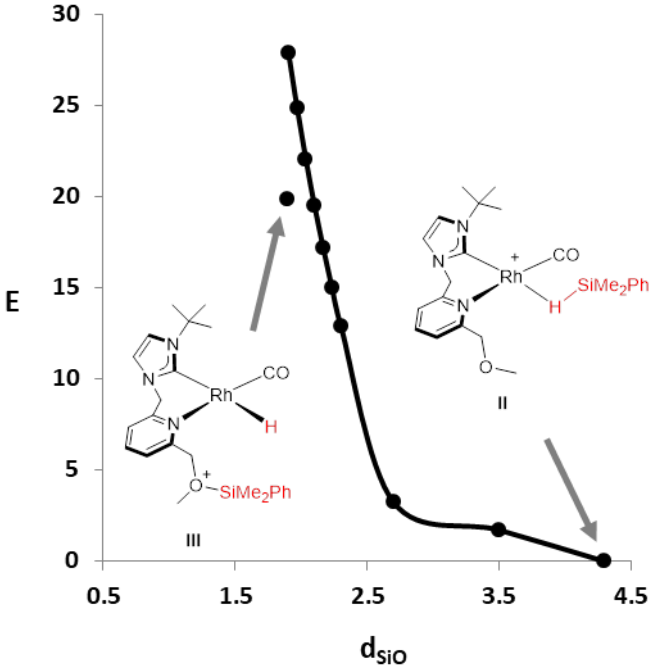

Figure S32. Energy (E, kcal·mol^{-1}) *vs*. Si⋯O distance (d_{SiO}, Å) for **II → III** (B97D3, def2svp, CPCM/$CHCl_3$, 298 K, 1 atm).